Int. J. Heat Mass Transfer. Vol. 26, No. 1, pp. 73–86, 1983
Printed in Great Britain

0017-9310/83/010073-14 $03.00/0

MIXED CONVECTION OVER A VERTICAL ZIRCALOY PLATE IN STEAM WITH SIMULTANEOUS OXIDATION

B. T. CHAO and S. J. CHEN
Department of Mechanical and Industrial Engineering, University of Illinois at Urbana-Champaign, Urbana, IL 61801, U.S.A.

and

L. S. YAO
Department of Mechanical and Energy Systems Engineering, Arizona State University, Tempe, AZ 85821, U.S.A.

(*Received* 15 *January* 1982 *and in final form* 9 *June* 1982)

Abstract—An analytical study is made of the quasi-steady, laminar, binary boundary layer flow of steam and hydrogen over a vertical Zircaloy plate under conditions pertinent to the Three Mile Island nuclear reactor accident. The experimentally observed oxidation rate law is modified to account for the possible presence of hydrogen in steam outside the boundary layer and for variable plate temperatures. The oxidation of Zircaloy gives rise to a small suction velocity of the steam–hydrogen mixture at the cladding surface. Details of the longitudinal and transverse components of the velocity profiles, temperature, and hydrogen concentration profiles across the binary boundary layer are presented as well as longitudinal distributions of wall suction velocity, wall shear, and wall temperature. A parametric study of the effect of surface radiative heat loss was made, using recently reported data on the radiation heat transfer coefficient. Correlations are proposed for the local wall temperature rise and for the local Nusselt and Sherwood numbers.

NOMENCLATURE

C_p, specific heat at constant pressure [kJ kg^{-1} K^{-1}];
$\overline{CR}$, chemical reaction parameter, $[(U_\infty k_\infty T_\infty)/(g\ q_{decay}\ \nu_\infty^2)]^{1/3}\ (1/\rho_\infty)\ (K/[\langle K\rangle\ t]^{1/2})$;
D, mass diffusivity [m^2 s^{-1}];
$f(Pr)$, Fujii's correlation function, equation (38);
$\bar{F}$, decay heat parameter, $[(q_{decay}/k_\infty T_\infty)^{2/3}]\ [(U_\infty \nu_\infty)/g)^{1/3}]$;
g, gravitational acceleration [m s^{-2}];
Gr_x, local Grashof number, $[g\ q_{decay}\ (5x)^4]/[\nu_\infty^2 k_\infty T_\infty]$;
h, heat transfer coefficient [W m^{-2} K^{-1}], h_c for convection, equation (32), h_r for radiation;
ΔH, heat of reaction [kJ kg^{-1}];
k, thermal conductivity [W m^{-1} K^{-1}];
K, parabolic rate constant [(kg m^{-2})^2 s^{-1}], $\langle K\rangle$ denotes mean value of K;
Nu_x, local Nusselt number, equation (33);
P, pressure [N m^{-2}];
Pr, Prandtl number, $C_p\ \mu/k$;
q, heat flux [W m^{-2}];
q_{decay}, heat flux due to fission product decay;
q_r, radiation heat flux;
q_{reac}, heat flux due to chemical reaction;
Re_x, local Reynolds number, $U_\infty\ 5x/\nu_\infty$;
$\overline{RP}$, radiation parameter, $(h_r\ T_\infty/q_{decay})\ \bar{F}\ \bar{s}^{1/3} = (2/5)^{1/2}\ (h_r\ 5x/k_\infty)\ Re_x^{-1/2}$;
$\bar{s}$, dimensionless axial coordinate, $(2/5)^{3/2}\ Gr_x/Re_x^{5/2} = 2(2\nu_\infty/U_\infty^5)^{1/2}\ (g\ q_{decay}/k_\infty T_\infty)\ x^{3/2}$;
Sc, Schmidt number, ν/D;
Sh_x, local Sherwood number, equation (44);
t, oxidation time [s];
T, temperature [K];
u, velocity component in x-direction [m s^{-1}];
$\bar{u}$, dimensionless velocity, u/U_∞;
U_∞, free stream velocity [m s^{-1}];
v, velocity component in y-direction [m s^{-1}];
$\bar{v}$, dimensionless velocity, $(2/5)^{1/2}\ (v/U_\infty)\ Re_x^{1/2}$;
x, coordinate along plate [m];
y, coordinate normal to plate [m].

Greek symbols

Δ, thickness of Zircaloy plate [m];
$\bar{\eta}$, dimensionless transverse coordinate, $(5/2)^{1/2}\ (y/5x)\ Re_x^{1/2}$;
$\bar{\theta}$, dimensionless temperature rise, $[(T/T_\infty) - 1]/\bar{F}\ \bar{s}^{1/3}$;
μ, dynamic viscosity [N s m^{-2}];
ν, kinematic viscosity [m^2 s^{-1}];
ρ, density [kg m^{-3}];
ω, hydrogen mass fraction;
$\bar{\omega}$, hydrogen mass fraction increase, $(\omega - \omega_\infty)/\bar{s}^{1/3}$.

Subscripts

1, refers to steam;
2, refers to hydrogen;
∞, refers to free stream;
w, refers to exterior surface of Zircaloy plate.

1. INTRODUCTION

ONE OF the problems frequently encountered in the safety analysis of a water reactor is the 'loss of coolant' accident (LOCA). During LOCA, the reactor core is gradually uncovered, and the residual water inventory is slowly boiled off by decay heating [1]. During the accident in the Unit 2 reactor of the Three Mile Island (TMI) nuclear power station, the core uncovery occurred about 100 min after the scram of the reactor [2]. At that time, the decay heating rate amounted to less than 1.5% of the full reactor power. Notwithstanding the low power level of decay heating, the temperature of the uncovered portion of the fuel rods would rise significantly due to the poor heat transfer capability of steam as compared to that of water. The hot Zircaloy cladding of the fuel rod reacts with steam to produce hydrogen while its mechanical strength deteriorates as oxidation proceeds. For the TMI-2 reactor, it was ascertained that the oxidation of the cladding had been developed to such an extent that radioactive gases leaked from the interior of the fuel rod and contaminated the primary coolant system. Hence, there is clear incentive to develop a model that is capable of predicting the oxidation rate of the Zircaloy cladding and the hydrogen generation rate under the slow boil-off condition. The phenomenon is complex because radiation will interact significantly with convection under the conditions of high pressure and temperature in the water reactor core [3]. No information about the extent of the effect of hydrogen generation in enhancing the buoyancy flow is available. Since the production of chemical reaction heat is strongly temperature dependent, its importance relative to the fission product decay heat can only be accurately assessed if the fuel rod cladding temperature is known. The latter would, in turn, depend upon the combined convective and radiative heat transport at the rod surface.

2. PHYSICAL MODEL AND GOVERNING EQUATIONS

Because of the rather complicated scenario of the TMI-2 LOCA, as a first step toward achieving some understanding of the physical and chemical processes involved, an idealized 2-dim. convection–radiation model was chosen for this study. It consists of a vertical Zircaloy flat plate with superheated steam flowing vertically upward past its hot surface as shown schematically in Fig. 1.† The coordinates along and normal to the plate are denoted by (x, y) and their

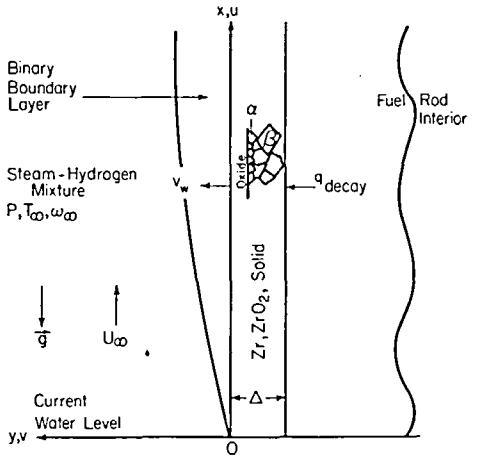

FIG. 1. Physical model and coordinate system (v_w is actually negative).

corresponding velocity components are (u, v). The origin of the coordinate system is chosen to coincide with the current water level. At the interior surface of the plate, there is a known heat flux, q_{decay}, due to fission products. At its exterior surface, dissociative chemisorption of steam molecules into oxygen and hydrogen ions or atoms takes place [4]. The combined effect of (i) the transport of steam toward the plate and across the boundary layer and (ii) the diffusion of oxygen through the oxide layer and subsequently in the α/β Zircaloy substrate results in a normal mixture velocity at the plate surface, v_w, which is actually negative. The boundary layer is a binary mixture of steam and hydrogen. The possible presence of a small amount of air and other gases is ignored. Outside the boundary layer, the steam flow is steady and has a free stream velocity U_∞, temperature T_∞, and hydrogen mass fraction ω_∞. For the TMI-2 conditions, the steam flow rate in the fuel rod bundle was reported to be 0.5 g s^{-1}/rod with dryout at the top of the core and to near zero as dryout was completed [4]. Based on the fuel assembly information made available to us [5], it was estimated that the upper limit of steam flow velocity in the channel was approximately 1.2 m s^{-1}. An estimation of the core uncovery history has been reported [2]. The coolant level receded from the normal 12 ft to 3 ft above the bottom of the core in 30–40 min and this occurred about 100 min after the turbine trip. A study of the phenomenon has been made [6] and it was concluded that a quasi-steady analysis is adequate for our present purpose.

Combined free and forced convection flow over a vertical flat plate with specified surface heat flux has been studied [7, 8]. These analyses are based on constant properties (except, of course, the change of density with temperature) and without radiation. It does not appear that information on mixed convection flow applicable to reactor core uncovering conditions is presently available. The case of pure free convection has been reported [9].

† The model is not intended for immediate reactor application for which channel flow in rod bundles must be considered.

2.1. *Governing equations and boundary conditions*

The governing conservation equations for the binary boundary layer motion are well known. For the convenience of the reader, they are given below in a form suitable for quasi-steady analysis.

Mixture continuity.

$$\partial(\rho u)/\partial x + \partial(\rho v)/\partial y = 0. \quad (1)$$

Mixture momentum.

$$[\rho\, u(\partial u/\partial x)] + [\rho\, v(\partial u/\partial y)] = (\rho_\infty - \rho)g + \partial(\mu\, \partial u/\partial y)/\partial y. \quad (2)$$

Mixture energy.

$$\rho C_p[(u\,\partial T/\partial x) + (v\,\partial T/\partial y)] = \partial(k\partial T/\partial y)/\partial y + \rho\, D(C_{p2} - C_{p1})(\partial T/\partial y)(\partial \omega/\partial y) - (\partial q_r/\partial y). \quad (3)$$

Conservation of hydrogen species.

$$\rho\, u(\partial \omega/\partial x) + \rho v(\partial \omega/\partial y) = \partial(\rho D\, \partial \omega/\partial y)/\partial y. \quad (4)$$

A rigorous evaluation of the radiative contribution, $\partial q_r/\partial y$ in equation (3), is quite complex because steam in fuel-rod bundles under uncovering conditions is in the intermediate regime of optical thickness [3]. Furthermore, the scattering of radiation by dispersed droplets may not be negligible [10]. Recognizing the difficulty and the uncertainty involved, it was decided not to seek a rigorous analysis but instead to assess the influence of radiation via an experimentally determined radiative heat transfer coefficient h_r for which some information has recently been made available [3]. Accordingly, in the analysis that follows, the term $\partial q_r/\partial y$ in equation (3) is deleted and a radiative heat flux $h_r(T_w - T_\infty)$ is incorporated into the thermal boundary condition. While this artifice will enable us to conduct a parametric study of the effect of radiation on the Zircaloy plate temperature, the field results, such as velocity and temperature distributions across the boundary layer, must necessarily be approximate. Furthermore, in interpreting the results, one must bear in mind that h_r is, in reality, strongly temperature dependent.

Boundary conditions.

$$\left.\begin{array}{l} x = 0,\ y > 0 \\ \quad \text{and} \\ y \to \infty \end{array}\right\} : u = U_\infty,\ T = T_\infty,\ \omega = \omega_\infty \quad (5a, b, c)$$

$$y = 0: \qquad u = 0,\ v = v_w(x, t). \quad (6a, b)$$

$$[-k(\partial T/\partial y)]_w = q_{decay} + q_{reac} - h_r(T_w - T_\infty). \quad (6c)$$

$$(D\,\partial \omega/\partial y)_w = [(1/8) + \omega_w]\, v_w. \quad (6d)$$

Equation (6c) follows an enthalpy balance of the Zircaloy plate† and equation (6d) is derived from the assumption that the dissociative chemisorption of steam into hydrogen and oxygen at the plate surface is stoichiometric. While the governing equations do not involve the time variable, v_w, q_{decay}, and q_{reac} in the boundary conditions are all time dependent, as is the solution. This is, of course, the consequence of the quasi-steady approximation for which the time variable becomes a parameter.

2.2. *Experimental laws for steam oxidation of Zircaloy*

The steam oxidation of Zircaloy follows the exothermic reaction

$$Zr + 2H_2O \rightarrow ZrO_2 + 2H_2 + \Delta H \quad (7)$$

where the heat of reaction ΔH is 6510 kJ kg^{-1}. A recent survey on the oxidation behavior of zirconium and Zircaloy is given in Appendix A of ref. [6]. A discontinuity in the reaction kinetics occurs as the specimen temperature is raised beyond approximately 1850 K, resulting in a sharp increase in the oxidation rate described as the breakaway phenomenon. Thus two oxidation regimes exist and are called pre-transition before breakaway and post-transition after breakaway. There is overwhelming evidence that under the condition of unlimited steam supply, pre-transition oxidation follows the parabolic law [6]

$$W^2 = Kt \quad (8)$$

where W is the mass of oxygen consumed per unit area of the exposed surface of Zircaloy during the teaction time t and K is the so-called parabolic rate constant expressible in terms of the Arrhenius equation

$$K = A \exp(-E/RT) \quad (9a)$$

in which A is an experimentally determined constant, E is the activation energy also determined experimentally and R is the universal gas constant, 8.314 kJ kmol^{-1} K^{-1}. Within the temperature range 1150–1850 K,

$$K\,[(\text{kg m}^{-2})^2\,\text{s}^{-1}] \simeq 3.82 \exp(-16800/T). \quad (9b)‡$$

The mass of total reacted zirconium (oxides and solid solutions) is 2.85 W.

The experimental oxidation law, equation (8), is established for constant temperature condition. For variable temperatures, it is rewritten as

$$dW/dt = K/2W \quad (10)$$

and if $W = 0$ when $t = 0$, as is usually the case, then

$$W^2 = \int_0^t K\, dt. \quad (11)$$

Combining equations (10) and (11) gives

$$dW/dt = (1/2)\, K/[\langle K\rangle t]^{1/2} \quad (12a)$$

†For the quasi-steady solution sought in this work, the thermal energy associated with heating up of the Zircaloy plate is approximately two orders of magnitude smaller than q_{decay} and is thus neglected.

‡A comparison of various expressions proposed is given in Appendix A of ref. [6].

in which $\langle K\rangle$ denotes the average value of K for the time duration $t = 0$ to $t = t$, i.e.

$$\langle K\rangle = t^{-1}\int_0^t K\,\mathrm{d}t. \tag{12b}$$

A consideration of the molar flux of steam arriving at the cladding surface due to combined diffusion and convection gives

$$\rho_w v_w = -(\mathrm{d}W/\mathrm{d}t) \tag{13a}$$

for the stoichiometric reaction depicted by equation (7). To account for the possible steam attribution in the free stream, equation (13a) is modified to read

$$\rho_w v_w = -c_w(\mathrm{d}W/\mathrm{d}t) = -(c_w/2)\,K/[\langle K\rangle t]^{1/2}$$
$$= -(1/2)\{1 + 9[\omega_w/(1-\omega_w)]\}^{-1}\,K/[\langle K\rangle t]^{1/2} \tag{13b}$$

where c_w is the local mole fraction of steam at the wall. The numeral 9 in equation (13b) is the ratio of the molecular weight of steam to that of hydrogen.

2.3. *Decay heat flux and oxidation heat flux*

The fission products decay heat has been extensively investigated. For a ^{235}U reactor after long-time operation, the ratio of the decay power to the normal operating power q_{oa} can be expressed as [11]

$$q_{decay}/q_{oa} = 0.1(t_s + 10)^{-0.2} - 0.087(t_s + 2\times 10^7)^{-0.2} - 0.0025\,\mathrm{e}^{-t_s/2040} - 0.0013\,\mathrm{e}^{-t_s/290\,000} \tag{14}$$

where t_s is the time in s after shutdown. The average normal operating power of the TMI-2 reactor is estimated to be

$$q_{oa} = 54\times 10^4\ \mathrm{W\,m^{-2}}. \tag{15}$$

The heat of oxidation can be conveniently expressed in terms of an equivalent surface heat flux q_{reac}. It is

$$q_{reac} = 2.85\,\Delta H(c_w/2)\,K/[\langle K\rangle t]^{1/2} \tag{16}$$

in which the numerical coefficient 2.85 is the ratio of the molecular weight of zirconium to that of oxygen. Based on the observation that the core uncovery occurs 100 min after the reactor scram, a detailed comparison of the decay heat with the exothermic chemical reaction heat has been made [6]. It was found that the chemical reaction heat is important only at the beginning of the oxidation process, particularly, at high fuel-rod temperatures. Its importance diminishes as time proceeds. At 10 min, it is less than 40% of the decay heat. Hence, for the quasi-steady solution sought, the normalizing parameters suitable for the nondimensionalization of the governing equations are those appropriate for a vertical plate with a uniform wall heat flux.

For the TMI-2 accident, the reactor cooling system pressure was reported to be 1075 and 625 psig, respectively for 80 min and 31 s and 137 min and 53 s after the scram of the reactor [2]. In this study, the system pressure was taken to be 6.9 MPa ($\simeq$ 1000 psig).

2.4. *Property evaluation*

Suitable methods are used for the evaluation of the relevant transport and thermodynamic properties of the steam–hydrogen mixture. The viscosity is based on a recommended procedure [12, 13], the thermal conductivity is adopted from ref. [14] and the binary mass diffusion coefficient is based on ref. [15]. Details, including a list of equations for density ratio ρ^* ($=\rho/\rho_\infty$), viscosity ratio μ^* ($=\mu/\mu_\infty$), thermal conductivity ratio k^*($=k/k_\infty$), specific heat ratio C_p^* ($=C_p/C_{p,\infty}$) and mass diffusivity ratio D^* ($=D/D_\infty$) can be found elsewhere [6].

2.5. *Transformed equations in parabolic coordinates* $(\bar{s}, \bar{\eta})$

Upon introducing the dimensionless parabolic coordinates $(\bar{s}, \bar{\eta})$ and other nondimensional quantities listed in the Nomenclature, equations (1)–(4) become

$$3\bar{s}\frac{\partial}{\partial\bar{s}}(\rho^*\,\bar{u}) - \bar{\eta}\frac{\partial}{\partial\bar{\eta}}(\rho^*\,\bar{u}) + \frac{\partial}{\partial\bar{\eta}}(\rho^*\,\bar{v}) = 0, \tag{17}$$

$$3\bar{u}\bar{s}\frac{\partial\bar{u}}{\partial\bar{s}} + (\bar{v} - \bar{u}\bar{\eta})\frac{\partial\bar{u}}{\partial\bar{\eta}} = \frac{1}{\rho^*}\frac{\partial}{\partial\bar{\eta}}\left(\mu^*\frac{\partial\bar{u}}{\partial\bar{\eta}}\right) + \{1 + [8/(1+8\omega_\infty)]\,\bar{s}^{1/3}\,\bar{\omega}\}\,\bar{s}\bar{\theta} + [8/(1+8\omega_\infty)]\,(1/\bar{F})\,\bar{s}\bar{\omega} \tag{18}$$

$$\left(3\bar{s}\frac{\partial\bar{\theta}}{\partial\bar{s}} + \bar{\theta}\right)\bar{u} + (\bar{v} - \bar{u}\,\bar{\eta})\frac{\partial\bar{\theta}}{\partial\bar{\eta}} = [1/(Pr_\infty C_p^*\,\rho^*)]\frac{\partial}{\partial\bar{\eta}}\left(k^*\frac{\partial\bar{\theta}}{\partial\bar{\eta}}\right) + \frac{1}{Sc_\infty}[(C_{p2}^* - C_{p1}^*)/C_p^*]\,D^*\,\bar{s}^{1/3}\frac{\partial\bar{\theta}}{\partial\bar{\eta}}\frac{\partial\bar{\omega}}{\partial\bar{\eta}}, \tag{19}$$

$$\left(3\,\bar{s}\frac{\partial\bar{\omega}}{\partial\bar{s}} + \bar{\omega}\right)\bar{u} + (\bar{v} - \bar{u}\,\bar{\eta})\frac{\partial\bar{\omega}}{\partial\bar{\eta}} = [1/(Sc_\infty\,\rho^*)]\frac{\partial}{\partial\bar{\eta}}\left(\rho^*\,D^*\frac{\partial\bar{\omega}}{\partial\bar{\eta}}\right). \tag{20}$$

The corresponding dimensionless boundary conditions are

For $\bar{\eta}\to\infty$

$$\bar{u} = 1,\quad \bar{\theta} = 0,\quad \text{and}\quad \bar{\omega} = 0 \tag{21, a, b, c}$$

For $\bar{\eta} = 0$

$$\bar{u} = 0 \tag{22a}$$

$$\bar{v}_w = -\frac{1}{2\rho_w^*}[(1 - \omega_\infty - \bar{s}^{1/3}\,\bar{\omega}_w)/(1 + 8\omega_\infty + 8\,\bar{s}^{1/3}\,\bar{\omega}_w)]\,\bar{s}^{1/3}\,\overline{CR} \tag{22b}$$

$$-k_w^*\frac{\partial\bar{\theta}}{\partial\bar{\eta}} = 1 + \frac{q_{reac}}{q_{decay}} - \overline{RP}\,\bar{\theta}_w \tag{22c}$$

$$\frac{\partial\bar{\omega}}{\partial\bar{\eta}} = -\frac{1}{16}[Sc_\infty/(\rho_w^*\,D_w^*)] \times (1 - \omega_\infty - \bar{s}^{1/3}\,\bar{\omega}_w)\,\overline{CR}. \tag{22d}$$

Table 1. Parameters $\overline{CR}$, $\bar{F}$ and $\overline{RP}$ for $P = 6.9$ MPa, $T_\infty = 1550$ K and $\omega_\infty = 0$

	U_∞ ($m\,s^{-1}$)	t (s) 60	600	3000	6000	300 000
$\overline{CR}$ †	0.1	0.245×10^{-1}	0.778×10^{-2}	0.357×10^{-2}	0.259×10^{-2}	0.493×10^{-3}
	1.0	0.527×10^{-1}	1.676×10^{-2}	0.770×10^{-2}	0.558×10^{-2}	1.061×10^{-3}
$\bar{F}$	0.1	0.349×10^{-1}	0.345×10^{-1}	0.327×10^{-1}	0.311×10^{-1}	0.172×10^{-1}
	1.0	0.753×10^{-1}	0.743×10^{-1}	0.705×10^{-1}	0.670×10^{-1}	0.371×10^{-1}
$\overline{RP}/\bar{s}^{1/3}$	0.1	0.535	0.540	0.553	0.568	0.762
($h_r = 70\,W\,m^{-2}\,K^{-1}$)	1.0	1.155	1.163	1.193	1.223	1.643

Both $\bar{F}$ and $\overline{RP}/\bar{s}^{1/3}$ are proportional to $U_\infty^{1/3}$.

† For estimation purpose, the parabolic rate constant K in $\overline{CR}$ is based on T_∞.

In equation (22c)

$$\frac{q_{reac}}{q_{decay}} = 1.425\,[(1 - \omega_\infty - \bar{s}^{1/3}\,\bar{\omega}_w)/(1 + 8\omega_\infty + 8\,\bar{s}^{1/3}\,\bar{\omega}_w)] \times [\Delta H/q_{decay}\,\{K/(\langle K\rangle\, t)^{1/2}\}] \quad (23)$$

The usual Boussinesq approximation is not used in the momentum equation (18). The use of the parabolic coordinates ($\bar{s}$, $\bar{\eta}$) serves the important function of removing the singularity at the leading edge. Since $\bar{s} = 0.253\,Gr_x/Re_x^{5/2}$, it provides a measure of the relative importance of free convection compared to forced convection in mixed flows. A small $\bar{s}$ is associated with forced convection dominated flow and a large $\bar{s}$ is associated with free convection dominated flow. This coordinate brings to bear the physics of the phenomenon under study. It stipulates a continuous transition from a perturbed forced convection flow in the region near the leading edge to a perturbed free convection flow in the region farther downstream.

The dimensionless parameters $\bar{F}$, $\overline{CR}$ and $\overline{RP}$ characterize, respectively, the role played by the fission product decay heat, chemical reaction heat and surface radiation loss. Their values for various times are shown in Table 1. All data are for $T_\infty = 1550$ K and $P = 6.9$ MPa ($\sim$ 1000 psig). It is seen that $\overline{CR}$ for $U_\infty = 0.1\,m\,s^{-1}$ is of the order 10^{-2} at $t = 60$ s and decreases to $O(10^{-3})$ at $t = 10^4$ s. At a given time, $\overline{CR} \propto U_\infty^{1/3}$. The parameter $\bar{F}$ is of $O(10^{-2})$ for $U_\infty = 0.1\,m\,s^{-1}$ and is insensitive to time variation; it also varies as $U_\infty^{1/3}$. The radiation parameter $\overline{RP}$ is evaluated for $h_r = 70\,W\,m^{-2}\,K^{-1}$ and is of $O(1)$ for $\bar{s} = 1$. It is directly proportional to h_r and varies as $\bar{s}^{1/3}$. Figure 2 shows that the effect of temperature and pressure on $\overline{CR}$ and $\bar{F}$ for $\omega_\infty = 0$, $U_\infty = 0.1\,m\,s^{-1}$ and oxidation time of 6000 s. Both $\overline{CR}$ and $\bar{F}$ are inversely proportional to $P^{1/3}$. At $P = 6.9$ MPa, $\overline{CR} \propto T^{0.352}$ and $\bar{F} \propto T^{-0.806}$. Other quantities in the governing equations have the following orders of magnitude:

(a) $\bar{u}$, $\bar{v}$, $\bar{\eta}$, $\bar{\theta}$, C_p^*, D^*, k^*, μ^* and ρ^* are all of $O(1)$,

(b) $\bar{\omega}$ is of $O(10^{-3}$–$10^{-4})$ as may be inferred from equation (22d).

In equation (18), $[8/(1 + 8\omega_\infty)]\,\bar{s}^{1/3}\,\bar{\omega}$ is ordinarily much less than unity, implying that the contribution to buoyancy due to the interaction of temperature and concentration gradients is negligible. The last term of equation (18) represents the direct contribution to buoyancy due to the presence of hydrogen. When $\bar{s} < 1$, it can also be ignored. It should be retained when $\bar{s} \gg 1$. In the vicinity of the leading edge, the local similarity solution is expected to hold. The governing conservation equations can be readily deduced from equations (17)–(20) by deleting terms involving the derivatives with respect to $\bar{s}$. If, furthermore, one restricts to the case of constant properties (except for density changes due to temperature differences) and without chemical reaction, the momentum and energy equations simplify to

$$\bar{f}''' + \bar{f}\bar{f}'' + \bar{s}\bar{\theta} = 0, \quad (24)$$

$$\bar{\theta}'' + Pr_\infty(\bar{f}\bar{\theta}' - \bar{\theta}\bar{f}') = 0 \quad (25)$$

where $\bar{f}(\bar{\eta})$ is a stream function defined by $\bar{u} = \bar{f}'$ and $\bar{v} = \bar{\eta}\bar{f}' - \bar{f}$, and the prime denotes differentiation with

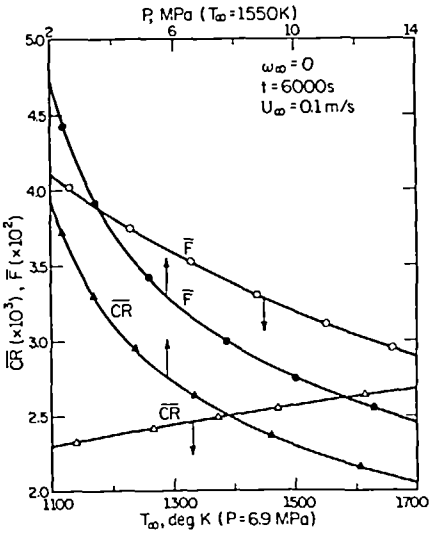

FIG. 2. Effect of temperature and pressure on parameters $\overline{CR}$ and $\bar{F}$.

respect to $\bar{\eta}$. Such is the case examined by Wilks [8]. Equations (24) and (25) are precisely those given in ref. [8] when the differences between the definitions for $\bar{s}$ and $\bar{\eta}$ and the parabolic coordinates used by Wilks are accounted for.

The parabolic oxidation rate constant K is governed by the plate temperature and hence it is also time dependent. The evaluation of $\langle K\rangle$, which appears in the chemical reaction parameter $\overline{CR}$ and in equation (23), requires that K be known at all times from $t = 0$ to $t = t$. For the quasi-steady solution sought, the oxidation time t should ideally be only a parameter if the simplicity of the quasi-steady analysis is to be preserved. Extensive calculation performed in the present study reveals that, except for very small times, the variation in K is limited and $[K/\langle K\rangle]^{1/2}$ does not differ much from unity, being slightly larger than 1 at earlier times and slightly less than 1 at later times. Hence, the following approximation is used in our numerical computation:

$$\frac{K}{[\langle K\rangle t]^{1/2}} = (K/\langle K\rangle)^{1/2}(K/t)^{1/2} \simeq (K/t)^{1/2} \quad (26)$$

which may be justified from the results of the numerical solution. We shall return to this point later.

Equations (17)–(20) with boundary conditions (21a, b, c) and (22a, b, c, d) were numerically integrated. The computer code MIXFLOW developed for this purpose is listed in Appendix C of ref. [6].

3. RESULTS AND DISCUSSION

In this section, sample results are presented for (a) the velocity, temperature, and hydrogen concentration profiles in the binary boundary layer, (b) the longitudinal distribution of wall suction velocity, local friction coefficient, wall temperature, wall hydrogen concentration, and local Nusselt number, and (c) the growth behavior of oxide layer with time. They are evaluated for $P = 6.9$ MPa ($\simeq$ 1000 psig), $T_\infty = 1550$ K, $\omega_\infty = 0$, $U_x = 0.1$ and 1.0 m s^{-1}, $\bar{s} = 0.15$ and 6.0, and two oxidation times of 600 and 6000 s. A parametric study of the effect of surface radiation was made for $h_r = 0$, 70, and 140 W m^{-2} K^{-1}. Additional results include those for $T_x = 1350$ K and $\omega_x = 0.9$. Correlations for the local wall temperature and the local Nusselt number of more general validity are developed. These correlations, though approximate are of the greatest interest in this study.

3.1. *Velocity profiles and wall shear distributions*

The longitudinal and normal velocity profiles for $U_x = 0.1$ m s^{-1} and $t = 600$ s are shown in Figs. 3(a) and (b), respectively. In interpreting the results, it is useful to recall that the physical velocities are related to the dimensionless velocities according to

$$u = \bar{u}U_x,$$

$$v = (5/2)^{1/2}\bar{v}U_x/Re_x^{1/2} = \bar{v}(U_x\nu_x/2x)^{1/2} = \bar{v}(g\nu_x\bar{F}/U_x)^{1/2}(\bar{s})^{-1/3}.$$

These figures and others presented in ref. [6] show that the effect of surface radiation on the velocity profiles is generally small at small $\bar{s}$ as expected, since the forced convection mechanism dominates there. As $\bar{s}$ increases, the contribution of buoyancy to the boundary layer flow increases and radiation exerts increasing influence. At $\bar{s} = 6.0$, the very strong effect of radiation is seen in both figures. As one approaches the edge of the boundary layer (large $\bar{\eta}$), the normal component of velocity tends to a constant for a given h_r, being positive for small $\bar{s}$ as typified by forced convection flow and negative for large $\bar{s}$ as typified by free convection flow.

While the influence of surface radiation on the $\bar{u}$-distribution is relatively small in the forced convection dominated region (small $\bar{s}$), its effect on the $\bar{v}$-distribution is greater. The reason for this is not immediately obvious and requires explanation. A close examination reveals that the phenomenon is mainly due to the effect of temperature change on the spatial rate of change of $\rho^*\bar{u}$, i.e. $\partial(\rho^*\bar{u})/\partial\bar{s}$, rather than the change in $\rho^*\bar{u}$ itself. This may be seen from the following. An integration of the continuity equation (17) from $\bar{\eta} = 0$ to $\bar{\eta} = \bar{\eta}$ gives

$$(\rho^*\bar{v})_{\bar{\eta}} - (\rho^*\bar{v})_w = \bar{\eta}(\rho^*\bar{u})_{\bar{\eta}} - \int_0^{\bar{\eta}} \rho^*\bar{u}\,d\bar{\eta} - 3\bar{s}\frac{\partial}{\partial\bar{s}}\int_0^{\bar{\eta}} \rho^*\bar{u}\,d\bar{\eta}. \quad (27)$$

Hence, for any $\bar{\eta} > 0$ where $(\rho^*\bar{v})_{\bar{\eta}} \gg (\rho^*\bar{v})_w$,

$$(\bar{v})_{\bar{\eta}} \simeq \bar{\eta}(\bar{u})_{\bar{\eta}} - \int_0^{\bar{\eta}} \frac{\rho^*}{(\rho^*)_{\bar{\eta}}}\bar{u}\,d\bar{\eta} - 3\bar{s}\frac{\partial}{\partial\bar{s}}\int_0^{\bar{\eta}} \frac{\rho^*}{(\rho^*)_{\bar{\eta}}}\bar{u}\,d\bar{\eta}. \quad (28)$$

A higher h_r would result in a lower temperature and hence a smaller $\bar{\theta}$ and a larger ρ^*. The concomitant smaller buoyancy force will bring forth a smaller $\bar{u}$. The resulting effect on $\rho^*\bar{u}/(\rho^*)_{\bar{\eta}}$ is such that it becomes greater. Had it not been for the last term in equation (28) which accounts for the non-similarity of the

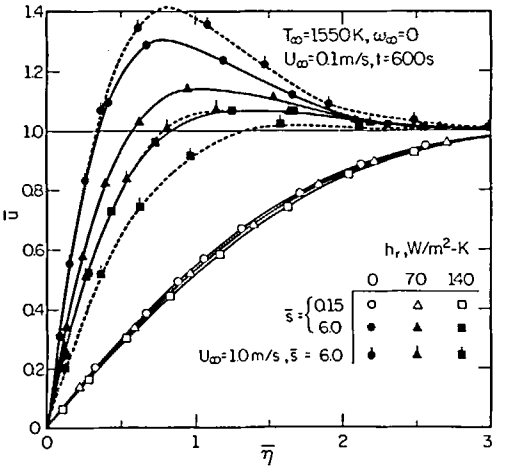

FIG. 3(a). Longitudinal velocity profiles in binary boundary layer for small and large $\bar{s}$.

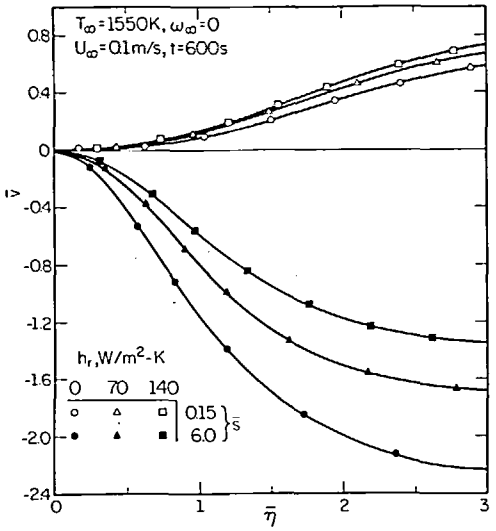

FIG. 3(b). Normal velocity profiles in binary boundary layer for small and large $\bar{s}$.

boundary layer flow, the net influence of a higher h_r would have been to produce a smaller $\bar{v}$ instead of a greater $\bar{v}$ as exhibited by the upper group of profiles in Fig. 3(b). A detailed study of the computer printout reveals that the contribution of the last term of equation (28) is indeed significant. An increase in h_r would result in a much smaller spatial rate of change of the integral

$$\int_0^{\bar{\eta}} \frac{\rho^*}{(\rho^*)_{\bar{\eta}}} \bar{u}\, d\bar{\eta}$$

with the net result that $\bar{v}$ is higher, including $\bar{v}_\delta$, the velocity at the edge of the boundary layer. In the free convection dominated region (large $\bar{s}$), the influence of surface radiation on the $\bar{v}$-distribution is similar to that for the pure free convection case [9].

The influence of free stream velocity on the $\bar{u}$- and $\bar{v}$-velocity profiles in the forced convection dominated region is relatively small, as one would again expect. However, in the free convection dominated region, significant effect is noted and the manner in which the velocity profiles change with U_∞ depends strongly on surface radiation. Included in Fig. 3(a) are three $\bar{u}$-distributions for $U_\infty = 1.0\,\mathrm{m\,s^{-1}}$. They are shown by

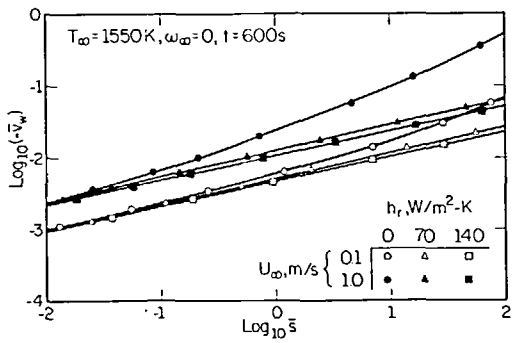

FIG. 4. Longitudinal distributions of wall suction velocity.

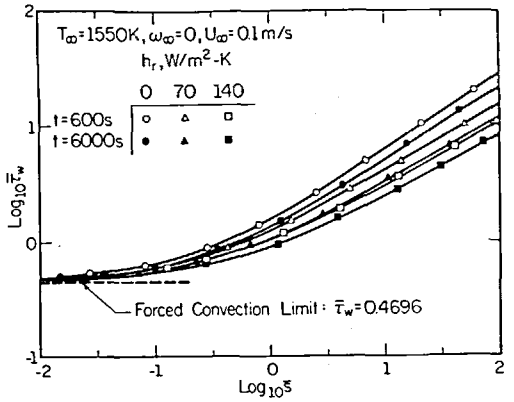

FIG. 5. Local skin friction coefficient.

the dotted curves. When h_r is zero, $\bar{u}$ is generally higher for larger U_∞. The reverse is true for $h_r = 70$ and $140\,\mathrm{W\,m^{-2}\,K^{-1}}$. This interesting phenomenon may be explained as follows. In the free convection dominated region, $\bar{u}^2$ is of the order of $\bar{s}\bar{\theta}$. Thus, for a given $\bar{s}$, $\bar{u}^2 \propto \bar{\theta}$. The dimensionless temperature $\bar{\theta}$ depends, among other things, on (a) q_{reac}/q_{decay} and (b) $\overline{RP}\,\bar{\theta}_w$ according to equation (22c). In the absence of surface radiation, $\overline{RP}$ vanishes and $\bar{\theta}$ depends on the chemical reaction heat alone. The latter is a function of the longitudinal distance x along the plate and it increases with increasing x. Now, at a given $\bar{s}$, $x \propto U_\infty^{5/3}$. Thus the chemical reaction heat for a fixed $\bar{s}$ is greater for $U_\infty = 1\,\mathrm{m\,s^{-1}}$ than for $U_\infty = 0.1\,\mathrm{m\,s^{-1}}$ and, consequently, both $\bar{\theta}$ and $\bar{u}$ increase with U_∞. In the presence of surface radiation, $\overline{RP} \propto U_\infty^{1/3}$ for a given h_r. As U_∞ increases from $0.1\,\mathrm{m\,s^{-1}}$ to $1\,\mathrm{m\,s^{-1}}$, surface radiation produces an effect on $\bar{\theta}$ opposite to that due to changing q_{reac}. The net result is a reduction in $\bar{\theta}$ and, hence, a reduction in $\bar{u}$ for higher U_∞.

The wall suction velocities produced by the steam oxidation of Zircaloy are generally small for the conditions studied. Their variations along the length of the plate are shown in Fig. 4. They increase with increasing $\bar{s}$ as indicated by equation (22b). The chemical reaction parameter $\overline{CR}$ also plays a role but its variation is relatively small since the reaction rate constant depends on the wall temperature in the absolute scale. At a given oxidation time, the wall suction velocity increases with U_∞ due to the higher chemical reaction rate; it decreases with increasing h_r as a result of the lower wall temperature. As time proceeds, the suction velocity decreases due to the lower wall temperature.

If, as is customary, one defines the local skin friction coefficient C_f as

$$C_f = \tau_w/(1/2\rho_\infty U_\infty^2) \tag{29}$$

where τ_w is the local wall shear, then

$$C_f\, Re_x^{1/2} = \sqrt{10}\,\bar{\tau}_w \tag{30}$$

where $\bar{\tau}_w = (\mu^*\,\partial\bar{u}/\partial\bar{\eta})_w$. Figure 5 shows the variation of the local skin friction coefficient expressed in terms

of $\bar{\tau}_w$ along the length of the plate. In the forced convection limit, $\bar{s} \to 0$, $\bar{\tau}_w = 0.4696$ which agrees with the well established result $C_f Re_x^{1/2} = 0.66412$ when Re_x is redefined as $U_\infty x/\nu_\infty$. As expected, $\bar{\tau}_w$ is higher for larger $\bar{s}$ as a result of increasing buoyancy force. At a given oxidation time, $\bar{\tau}_w$ decreases with increasing h_r; and at a given h_r, $\bar{\tau}_w$ decreases with increasing oxidation time. These are the consequence of lower wall temperature and hence lower fluid viscosity and lower suction velocity. In both the mixed and free convection dominated regions, $\bar{\tau}_w$ is higher for greater U_∞ under otherwise identical conditions.

3.2. *Temperature profiles and wall temperature distributions*

The temperature distributions in the boundary layer are illustrated in Fig. 6 for $U_\infty = 0.1$ and $1.0\,\mathrm{m\,s^{-1}}$. The dimensionless temperature $\bar{\theta}$ is related to the temperature difference $(T - T_\infty)$ according to

$$T - T_\infty = T_\infty \bar{F} \bar{s}^{1/3} \bar{\theta}$$

$$= (q_{decay}/k_\infty)^{2/3} (T_\infty U_\infty \nu_\infty/g)^{1/3} \bar{s}^{1/3} \bar{\theta}.$$

It is seen that the surface radiation has a significant effect, particularly on the wall temperatures. In all cases, $\bar{\theta}$ is smaller for higher h_r as one would expect. However, the influence of free stream velocity is rather complicated. When $h_r = 0$, $\bar{\theta}$ is greater for higher U_∞. The reverse is true for $h_r = 70$ and $140\,\mathrm{W\,m^{-2}\,K^{-1}}$. This phenomenon persists for both $\bar{s} = 0.15$ and 6.0 and can be explained as follows. If one ignores the variation of k_w^* due to changes in T_w as a result of changing U_∞, equation (22c) may be approximated by

$$\bar{\theta}_w \simeq [1 + (q_{reac}/q_{decay}) - \overline{RP}\,\bar{\theta}_w]\,\bar{\eta}_t \quad (31a)$$

where $\bar{\eta}_t$ is the dimensionless thermal boundary layer thickness. Equation (31a) may be rewritten as,

$$\bar{\theta}_w \simeq [1 + (q_{reac}/q_{decay})]\,\bar{\eta}_t/(1 + \overline{RP}\,\bar{\eta}_t). \quad (31b)$$

As has been pointed out in Section 3.1, the chemical reaction heat q_{reac} increases with increasing x and for a given $\bar{s}$, $x \propto U_\infty^{5/3}$. Thus, q_{reac} is greater for $U_\infty = 1.0\,\mathrm{m\,s^{-1}}$ than for $U_\infty = 0.1\,\mathrm{m\,s^{-1}}$. When $h_r = 0$, $\overline{RP} = 0$, and $\bar{\theta}_w \simeq [1 + (q_{reac}/q_{decay})]\,\bar{\eta}_t$. Hence, for a fixed $\bar{s}$, $\bar{\theta}_w$ for $U_\infty = 1.0\,\mathrm{m\,s^{-1}}$ is greater than $\bar{\theta}_w$ for $U_\infty = 0.1\,\mathrm{m\,s^{-1}}$. When $h_r \neq 0$, $\overline{RP} \propto U_\infty^{1/3}$ for a fixed $\bar{s}$. As U_∞ changes from 0.1 to $1.0\,\mathrm{m\,s^{-1}}$, the increase in the denominator of equation (31b) is larger than the increase in its numerator, resulting in a reduction of $\bar{\theta}_w$.

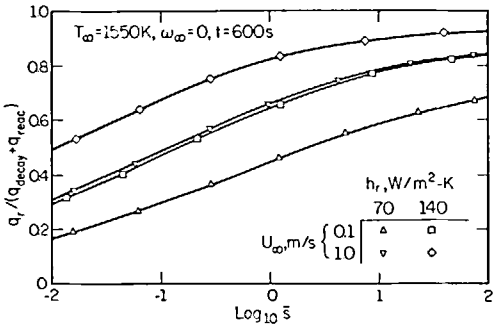

FIG. 7. Variations of heat flux ratio along plate.

The variations of the ratio of radiative flux to the sum of the fission product decay and chemical reaction heat flux along the length of the plate are displayed in Fig. 7 for $U_\infty = 0.1$ and $1.0\,\mathrm{m\,s^{-1}}$ and for $t = 600$ s. The corresponding curves for $t = 6000$ s are slightly higher. The increase of this ratio with increasing $\bar{s}$ is understandable. Just as in the case of pure free convection, the plate temperature increases with distance from the leading edge and both q_r and q_{reac} increase while q_{decay} remains constant. The increase in q_r is greater than that of q_{reac}, giving rise to the general trend of the curves shown. As U_∞ changes from 0.1 to $1.0\,\mathrm{m\,s^{-1}}$ $(T_w - T_\infty)$ at a given $\bar{s}$, increases even though $\bar{\theta}_w$ decreases, resulting in an increase in q_r that is greater than that of q_{reac}. The end result is that the ratio increases with U_∞.

The variations of the dimensionless wall temperature $\bar{\theta}_w$ with $\bar{s}$ are shown in Fig. 8 for $t = 600$ s. It is seen that $\bar{\theta}_w$ decreases with increasing h_r, as expected. Other trends may be explained as follows. As $\bar{s} \to 0$, $\overline{RP} \to 0$, i.e. the effect of surface radiation vanishes. This corresponds to the case of *pure* forced convection over a

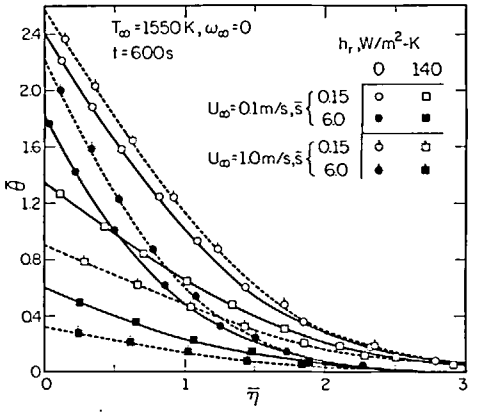

FIG. 6. Temperature profiles in binary boundary layer for small and large $\bar{s}$.

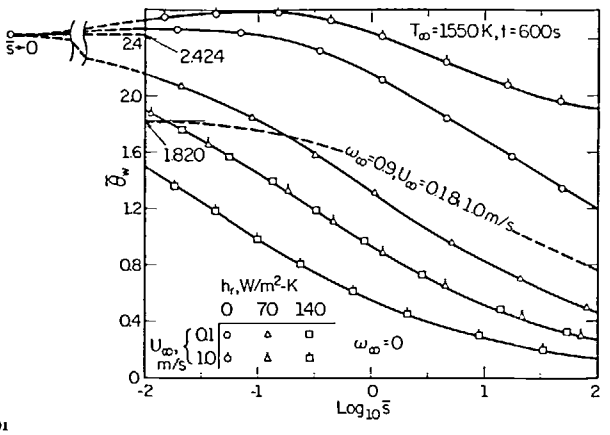

FIG. 8. Wall temperature distribution along plate.

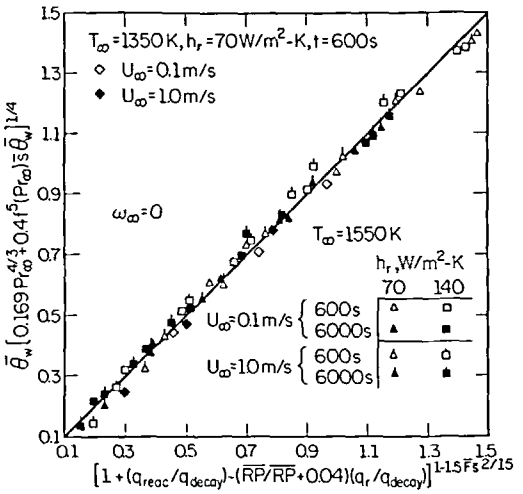

FIG. 9. Proposed wall temperature correlation in the presence of surface radiation ($\bar{s}$ ranges from 0 to 100).

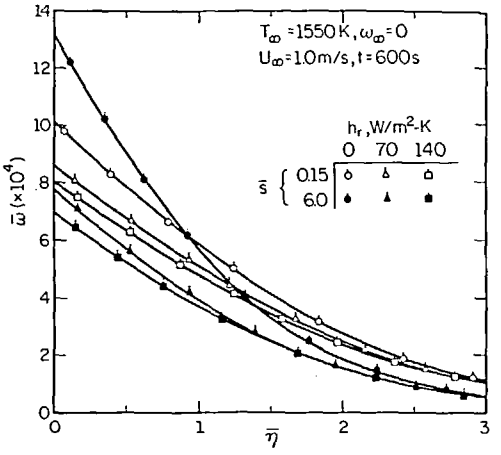

FIG. 11. Hydrogen concentration profiles in binary boundary layer for small and large $\bar{s}$.

flat plate with uniform wall heat flux for which $Nu_x/Re_x^{1/2}$ = constant for a given Prandtl number. This agrees with our present finding that for $\omega_\infty = 0$, ($Pr_\infty = 0.816$),

$$\bar{\theta}_w|_{\bar{s}\to 0} = 2.424 \text{ for } t = 600\text{ s}$$

which is independent of U_∞. Hence, if one extends all curves (except for $\omega_\infty = 0.9$) exhibited in Fig. 8 towards

$$\bar{s} = 0\ (\log_{10}\bar{s}|_{\bar{s}=0} = -\infty),$$

they converge to one point as illustrated. When $h_r = 0$, $\bar{\theta}_w$ increases with $\bar{s}$ for small $\bar{s}$ due to the increasing chemical reaction heat. At the same time, the buoyancy force exerts an increasingly important role in affecting the heat and mass transfer processes. Because of these two opposing factors, $\bar{\theta}_w$ reaches a maximum and it decreases with further increase in $\bar{s}$ as the free convection effect assumes its importance. When $h_r = 70$ and 140 W m^{-2} K^{-1}, the just described maximum is completely suppressed and $\bar{\theta}_w$ exhibits a monotonous decrease as $\bar{s}$ increases. Furthermore, $\bar{\theta}_w$ is smaller for higher U_∞. These observations are completely consistent with equation (31b).

Included in the figure are the results for $\omega_\infty = 0.9$, $h_r = 0$ and $U_\infty = 0.1$ and 1.0 m s^{-1}. Other things being

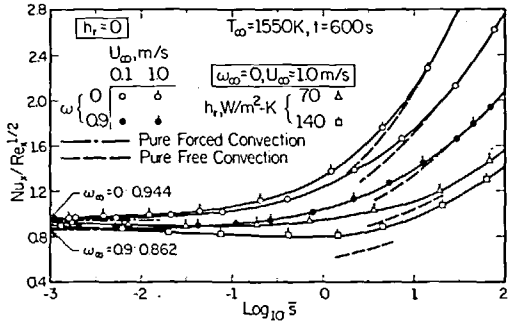

FIG. 10. Variations of $Nu_x/Re_x^{1/2}$ along plate.

equal, $\bar{\theta}_w$ is lower when compared to the case of $\omega_\infty = 0$ because of the much reduced chemical reaction heat. Furthermore, data for $U_\infty = 0.1$ and 1.0 m s^{-1} lie very closely in a single curve as illustrated, behaving very much like a single component fluid of constant properties. We shall return to this point later.

3.3. *Development of correlations for local wall temperature and local Nusselt number*

In an attempt to develop a correlation for $\bar{\theta}_w$, we proceed by establishing two limiting forms: one is valid for $\bar{s} \to 0$ where the heat transfer is by forced convection only and another for large $\bar{s}$ where the heat transfer is essentially by free convection.

Defining the mixed convection coefficient h_c in the usual way,

$$q_{decay}[1 + (q_{reac}/q_{decay}) - (q_r/q_{decay})] = h_c(T_w - T_\infty) \quad (32)$$

and the corresponding local Nusselt number by

$$Nu_x = \frac{h_c\, 5x}{k_\infty}, \quad (33)$$

we find

$$(2/5)^{1/2}(Nu_x/Re_x^{1/2})\bar{\theta}_w = 1 + (q_{reac}/q_{decay}) - (q_r/q_{decay}) \quad (34)$$

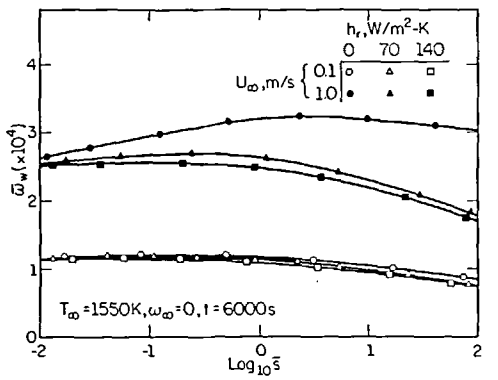

FIG. 12. Variation of surface hydrogen concentration along plate.

since $(T_w - T_\infty) = T_\infty \theta_w \bar{F} \bar{s}^{1/3}$ and $\bar{F}\bar{s}^{1/3} = (2/5)^{1/2} Re_x^{-1/2} (5x)(q_{decay}/k_\infty T_\infty)$.

As $\bar{s} \to 0$, $\overline{RP} \to 0$ and in the absence of chemical reaction, the case reduces to that of pure forced convection along a flat plate of uniform wall heat flux for which Kays [16] gave

$$Nu_x/Re_x^{1/2} = 1.01\, Pr^{1/3} \tag{35}$$

when the difference in the reference length used in Nu_x and Re_x is accounted for. Hence, in the forced convection limit, we have

$$0.641\, Pr^{1/3} \theta_{w,\bar{s}\to 0} = 1 + (q_{reac}/q_{decay}). \tag{36}$$

For large $\bar{s}$, the wall temperature is given in ref. [9]. Using the Nomenclature of this paper, it is

$$\theta_{w,\text{large }\bar{s}} \left[\frac{2}{5} f^5(Pr_\infty)\, \bar{s}\, \theta_{w,\text{large }\bar{s}}\right]^{1/4} = [1 + (q_{reac}/q_{decay}) - (q_r/q_{decay})]^{1-(5/4)(5/2)^{1/3}\bar{F}\bar{s}^{2/15}} \tag{37}$$

where $f(Pr)$ is Fujii's Prandtl number function for Nusselt number correlation [17]. It is defined by

$$f(Pr) = [5\, Pr^2/(4 + 9\, Pr^{1/2} + 10\, Pr)]^{1/5}. \tag{38}$$

A simple correlation that satisfies both limiting forms is

$$\theta_w[0.169\, Pr_\infty^{4/3} + 0.4 f^5(Pr_\infty)\, \bar{s}\, \theta_w]^{1/4} = \{1 + (q_{reac}/q_{decay}) - [\overline{RP}/(\overline{RP} + 0.04)](q_r/q_{decay})\}^{1-1.5\bar{F}\bar{s}^{2/15}}. \tag{39}$$

We note that $0.169^{1/4} = 0.641$ and $(5/4)(5/2)^{1/5} = 1.5$. The empirical modification factor $\overline{RP}/(\overline{RP} + 0.04)$ is introduced to improve the agreement between equation (39) and the solution data calculated from the computer code for a very wide range of conditions. Figure 9 demonstrates the usefulness of the proposed correlation. Since the parabolic oxidation rate law, equation (9b), is valid for 1150–1850 K, the use of equation (39) must necessarily be limited to the same temperature range.

Since,

$$\left(-k^* \frac{\partial \theta}{\partial \bar{\eta}}\right)_w = 1 + \frac{q_{reac}}{q_{decay}} - \frac{q_r}{q_{decay}}, \tag{40}$$

one has from equation (34),

$$\frac{Nu_x}{Re_x^{1/2}} = (5/2)^{1/2} \frac{1}{\theta_w} \left(-k^* \frac{\partial \theta}{\partial \bar{\eta}}\right)_w. \tag{41}$$

Results for $Nu_x/Re_x^{1/2}$ as evaluated from equation (41) are shown in Fig. 10. As $\bar{s} \to 0$, the forced convection limits determined from equation (35) are: $Nu_x/Re_x^{1/2} = 0.944$ for $\omega_\infty = 0$ ($Pr_\infty = 0.816$) and 0.862 for $\omega_\infty = 0.9$ ($Pr_\infty = 0.622$). These are shown by the dash-dot straight lines. The free convection limits appropriate for large $\bar{s}$ are shown by the dashed curves. In the absence of radiation and $\omega_\infty = 0$, the ratio $Nu_x/Re_x^{1/2}$ is higher for larger U_∞ and the effect of increasing U_∞ becomes more prominent for large $\bar{s}$. Again, the reason is due to the higher chemical reaction heat associated with larger U_∞. For a given $\bar{s}$, $x \propto U_\infty^{5/3}$ and q_{reac} increases with increasing x. When $\omega_\infty = 0.9$, this effect, to a very large extent, disappears due to the greatly reduced chemical reaction heat. For a single component fluid, $\omega_\infty = 1.0$ and hence $q_{reac} = 0$, equation (40) shows that, in the absence of radiation, $[-k^*(\partial\theta/\partial\bar{\eta})]_w = 1$. Under these conditions, equation (41) gives

$$\theta_w = (5/2)^{1/2}[(Re_x^{1/2})/(Nu_x)] \tag{41a}$$

which is a function of $\bar{s}$ alone and is independent of U_∞ as was pointed out in refs. [7, 8], both of which assumed constant properties. The dashed curve in Fig. 8 indicates that, for all practical purposes, the same conclusion holds for $\omega_\infty = 0.9$ and for variable properties.

When $h_r = 70$ or 140 W m^{-2} K^{-1}, the data for $Nu_x/Re_x^{1/2}$ exhibit a slight drop with increasing $\bar{s}$, reaching a minimum and then increasing with further increase in $\bar{s}$. In the forced convection dominated region (small $\bar{s}$), the reduction in wall heat flux due to the surface radiation loss more than compensates for the reduction in wall temperature, resulting in a drop in the local Nusselt number. In the free convection dominated region (large $\bar{s}$), the phenomenon reverses itself due to the increasingly important role of the buoyancy effect.

3.4. *Hydrogen concentration profiles and wall concentration distributions*

The hydrogen concentration profiles across the boundary layer are shown in Fig. 11 for $U_\infty = 1.0$ m s^{-1}. The dimensionless hydrogen mass fraction $\bar{\omega}$ is related for the mass fraction difference $\omega - \omega_\infty$ in accordance with

$$\omega - \omega_\infty = \bar{s}^{1/3} \bar{\omega}.$$

As in the case of pure free convection, $\omega - \omega_\infty$ is very small. It is of the order 10^{-3} or 10^{-4}. Consequently, the hydrogen flow in the boundary layer has only very minor direct influence on heat transfer. The heat and mass transfer processes are essentially decoupled. In the forced convection dominated region, $\bar{\omega}$ is lower for higher h_r, as expected, due to lower wall temperature. In the free convection dominated region, the trend persists when $U_\infty = 1.0$ m s^{-1} as exhibited in Fig. 11. However, when $U_\infty = 0.1$ m s^{-1}, the $\bar{\omega}$ vs $\bar{\eta}$ plots for $h_r = 0$, 70 and 140 W m^{-2} K^{-1} cross each other—a phenomenon similar to that for pure free convection [9].

Variations of wall hydrogen concentration along the plate are shown in Fig. 12 for oxidation time of 6000 s. Results for $t = 600$ s (not shown in figure) are 3–4 times greater. The reason is, of course, due to the slowing down of the chemical reaction rate and the reduction of decay heating as time proceeds. All data for $\bar{\omega}_w$ shown in Fig. 12 and others evaluated for $t =$

600 s, and also for $T_\infty = 1350$ K can be correlated by the following empirical equation:

$$\{16\,\bar{\omega}_w/[Sc_\alpha(1-\omega_\infty)\overline{CR}]\}\,[1+(0.2\,\overline{RP}\,\bar{\theta}_w^{1/2}/\bar{s}^{1/3})] = \bar{\theta}_w\,(Pr_\alpha/Sc_\alpha)^n\,[1+(q_{reac}/q_{decay})-(q_r/q_{decay})]^{-1} \quad (42)$$

where n is given by

$$n = \tfrac{1}{3} + [0.435\,\overline{CR}_\infty\,\bar{s}^{1/2}/(\overline{CR}_\infty\,\bar{s}^{1/2} + 0.85\,\bar{F}^{1/2})] \quad (42a)$$

We note that as $\bar{s} \to 0$, both $\overline{RP}\,\bar{\theta}_w^{1/2}/\bar{s}^{1/3}$ and $\overline{CR}_\infty\,\bar{s}^{1/2}/(\overline{CR}_\infty\,\bar{s}^{1/2} + 0.85\,\bar{F}^{1/2})$ vanish. Ref. [6] provides evidence demonstrating the usefulness of equation (42).

Equation (42) may be rewritten as

$$\{(16\,\bar{\omega}_w)/[Sc_\alpha(1-\omega_\infty)\overline{CR}]\}\,[1+(0.2\,\overline{RP}\,\bar{\theta}_w^{1/2}/\bar{s}^{1/3})] = (5/2)^{1/2}\,(Re_x^{1/2}/Nu_x)\,(Pr_\alpha/Sc_\alpha)^n \quad (43)$$

by using equation (34).

If one defines a local Sherwood number by

$$Sh_x = h_m\,5x/(\rho_\infty D_\infty) \quad (44)$$

in which h_m is the local mass transfer coefficient given by

$$h_m(\omega_w - \omega_\infty) = -\left(\rho D\frac{\partial\omega}{\partial y}\right)_w \quad (45)$$

then

$$Sh_x/Re_x^{1/2} = (5/2)^{1/2}\,(\bar{\omega}_w)^{-1}\left(-\rho^* D^*\frac{\partial\bar{\omega}}{\partial\bar{\eta}}\right)_w = \frac{1}{16}(5/2)^{1/2}\,(\bar{\omega}_w)^{-1}\,Sc_\infty\,(1-\omega_\infty-\bar{s}^{1/3}\,\bar{\omega}_w)\,\overline{CR} \simeq \frac{1}{16}(5/2)^{1/2}\,(\bar{\omega}_w)^{-1}\,Sc_\infty\,(1-\omega_\infty)\,\overline{CR} \quad (46)$$

since $\bar{s}^{1/3}\,\bar{\omega}_w \ll (1-\omega_\infty)$ unless ω_∞ is close to unity.

Equations (43) and (46) may be combined to give

$$Sh_x/Nu_x = (Sc_\alpha/Pr_\alpha)^n\,[1+(0.2\,\overline{RP}\,\bar{\theta}_w^{1/2}/\bar{s}^{1/3})]. \quad (47)$$

The variations in mixture material properties, ρ^*, C_p^*, μ^*, k^* and D^* are illustrated in Fig. 13 for $U_\infty = 0.1\ \mathrm{m\,s^{-1}}$. As expected, the variations are generally smaller in the forced convection dominated region. For a given $\bar{s}$, increasing U_∞ accentuates the variation because of the higher wall temperature at greater x.

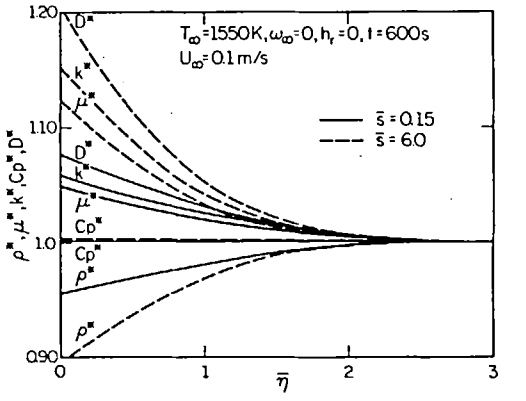

FIG. 13. Variations of mixture properties across binary boundary layer for small and large $\bar{s}$.

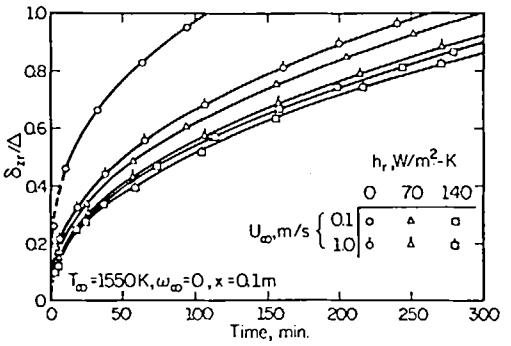

FIG. 14. Growth of oxidized Zircaloy layer with time (Δ = 6.73 × 10^{-4} m).

The variations in mixture material properties, ρ^*, C_p^*, μ^*, k^* and D^* are illustrated in Fig. 13 for $U_\infty = 0.1\ \mathrm{m\,s^{-1}}$. As expected, the variations are generally smaller in the forced convection dominated region. For a given $\bar{s}$, increasing U_∞ accentuates the variation because of the higher wall temperature at greater x.

3.5. *Hydrogen generation rate and thickness of reacted Zircaloy*

At any given location and time, once the wall temperature is known, the parabolic rate constant follows immediately from equation (9b) and, thence, the local hydrogen mass flux can be calculated from the following equation:

$$\dot{m}_{H_2} = \rho_w\,v_w\,\omega_w - \left(\rho D\frac{\partial\omega}{\partial y}\right)_w = \frac{1}{16}[(1-\omega_w)/(1+8\omega_w)]\,\{K/(\langle K\rangle t)^{1/2}\} \quad (48a)$$

$$\simeq \frac{1}{16}[(1-\omega_\infty)/(1+8\omega_x)]\,(K/t)^{1/2}. \quad (48b)$$

The growth rate of the reacted Zircaloy layer is

$$\frac{d\delta_{Zr}}{dt} = \frac{1}{32}[(1-\omega_w)/(1+8\omega_w)] \times (M_{Zr}/M_{H_2})(1/\rho_{Zr})\,\{K/(\langle K\rangle t)^{1/2}\} \quad (49a)$$

$$\simeq 2.2\times10^{-4}[(1-\omega_\infty)/(1+8\omega_\infty)]\,(K/t)^{1/2}. \quad (49b)$$

In deriving equation (49b), ρ_{Zr} is taken to be 6490 kg m^{-3} and the molecular weight of zirconium M_{Zr} and that of hydrogen M_{H_2} are 91.22 and 2.0, respectively. Equation (49b) was numerically integrated to obtain the thickness of the reacted Zircaloy layer as time proceeds. The results are illustrated in Fig. 14 for the location $x = 0.1$ m. Since q_{decay} varies with time, the corresponding $\bar{s}$ also varies with time as shown in Table 2. Included in the table are the local Reynolds and Grashof numbers, the local wall temperature and the associated parabolic oxidation rate constant K. The variation in K from $t = 600$ s to 6000 s

Table 2. Values of $\bar{s}$, Gr_x, T_w, and K corresponding to several combinations of U_∞ and x ($T_\infty = 1500\,\mathrm{K}$, $\omega_\infty = 0$, $h_r = 70\,\mathrm{W\,m^{-2}\,K^{-1}}$)

		t(s)				
		60	600	3000	6000	300 000
	$q_{decay}(\mathrm{W\,m^{-2}})$	7072	6930	6414	5945	2450
$U_\infty = 0.1\,\mathrm{m\,s^{-1}}$						
$x = 0.1\,\mathrm{m}$						
$(Re_x = 7.87\times10^3)$						
	$\bar{s}$	17.9	17.6	16.2	15.1	6.2
	Gr_x	3.89×10^{11}	3.81×10^{11}	3.53×10^{11}	3.27×10^{11}	1.35×10^{11}
	T_w(K)	1757	1649	1624	1615	1575
	$K[(\mathrm{kg\,m^{-2}})^2/\mathrm{s}]$	2.68×10^{-4}	1.43×10^{-4}	1.22×10^{-4}	1.16×10^{-4}	0.89×10^{-4}
$x = 0.3\,\mathrm{m}$						
$(Re_x = 2.36\times10^4)$						
	$\bar{s}$	93.1	91.2	84.4	78.3	32.3
	Gr_x	3.15×10^{13}	3.09×10^{13}	2.86×10^{13}	2.65×10^{13}	1.10×10^{13}
	T_w(K)	1797	1661	1632	1622	1578
	$K[(\mathrm{kg\,m^{-2}})^2/\mathrm{s}]$	3.32×10^{-4}	1.54×10^{-4}	1.29×10^{-4}	1.21×10^{-4}	0.90×10^{-4}
$U_\infty = 1.0\,\mathrm{m\,s^{-1}}$						
$x = 0.1\,\mathrm{m}$						
$(Re_x = 7.87\times10^4)$						
	$\bar{s}$	0.057	0.056	0.051	0.048	0.020
	Gr_x	3.89×10^{11}	3.81×10^{11}	3.53×10^{11}	3.27×10^{11}	1.35×10^{11}
	T_w(K)	1690	1619	1602	1595	1567
	$K[(\mathrm{kg\,m^{-2}})^2/\mathrm{s}]$	1.83×10^{-4}	1.19×10^{-4}	1.06×10^{-4}	1.02×10^{-4}	0.84×10^{-4}
$x = 1.0\,\mathrm{m}$						
$(Re_x = 7.87\times10^5)$						
	$\bar{s}$	1.79	1.76	1.62	1.51	0.62
	Gr_x	3.89×10^{15}	3.81×10^{15}	3.53×10^{15}	3.27×10^{15}	1.35×10^{15}
	T_w(K)	1834	1667	1635	1624	1577
	$K[(\mathrm{kg\,m^{-2}})^2/\mathrm{s}]$	4.00×10^{-4}	1.60×10^{-4}	1.31×10^{-4}	1.23×10^{-4}	0.90×10^{-4}

The reference length used in Re_x and Gr_x is $5x$. Hence, the above tabulated values for Re_x and Gr_x should be reduced, respectively, by a factor of 5 and 5^4 ($=625$) if x is selected for the reference length.

or even 300 000 s is limited and hence $[K/\langle K\rangle]^{1/2} \simeq 1$, justifying the approximation introduced in equation (26). Such approximation is clearly unwarranted for oxidation times much less than 600 s. When t is less than 60 s, the quasi-steady solution would also become invalid. The data of Table 2 suggest that the binary boundary layer flow at $x = 0.1$ m is dominated by free convection when $U_\infty = 0.1\,\mathrm{m\,s^{-1}}$ ($\bar{s}$ ranges from 17.9 at 60 s to 6.2 at 300 000 s). This is in contrast with the forced convection dominated flow when $U_\infty = 1.0\,\mathrm{m\,s^{-1}}$ ($\bar{s}$ ranges from 0.057 at 60 s to 0.020 at 300 000 s). Had the reference length in Gr_x been x instead of $5x$ as defined in the Nomenclature, its value at 600 s would be 6.1×10^8. Hence, at $x = 0.1$ m, the boundary layer flow is expected to be laminar even when $U_\infty = 0.1\,\mathrm{m\,s^{-1}}$. Figure 14 shows that the growth rate of the oxidized layer is significantly affected by surface radiation, as expected. Other things being equal, the thickness of the oxidized layer is greater for $U_\infty = 0.1\,\mathrm{m\,s^{-1}}$ than it is for $U_\infty = 1.0\,\mathrm{m\,s^{-1}}$ due to the higher plate temperature. The difference, however, becomes less as h_r increases. This is attributed to the manner by which the parabolic oxidation rate constant depends on the plate temperature at the level of temperature considered. Because of the uncertainty in the results for small times, all curves are shown dotted for t less than 5 min.

Growth curves for $x = 0.3$ m and $U_\infty = 0.1\,\mathrm{m\,s^{-1}}$ and for $x = 1.0$ m and $U_\infty = 1.0\,\mathrm{m\,s^{-1}}$ have been obtained and are presented in ref. [6]. Because of the magnitude of Gr_x involved, the boundary layer flow would most likely be turbulent in both instances. If this were indeed the case, the results would obviously not be valid, since the present analysis is based on the laminar flow assumption. There is a dearth of information on the criterion for the boundary layer flow to be laminar or turbulent even for the simple case of a single component fluid and without chemical reaction. For an isothermal plate in air, Hall and Price [18] reported the interesting effect of an aiding forced flow on a turbulent free convection boundary layer. As the forced flow velocity is increased, the heat transfer coefficient initially decreases and then increases. The initial decrease coincides with the lower turbulence intensity in the free convection boundary layer. This seems to suggest that, within limit, the presence of an aiding forced flow would delay the transition to turbulence. More work, both experimental and analytical, needs to be done on the subject.

For reactor applications, the single flat plate geometry is clearly unrealistic and vertical channel flow must be considered. Because of the very small diameter-to-length ratio associated with reactor coolant channels (of the order 10^{-2}–10^{-3}), transition to turbulence is expected to be delayed significantly or may even be suppressed.

Acknowledgements—The authors express their appreciation to the Electric Power Research Institute for the support of this research under Contract EPRI RP 1760-2 and to Dr Bill K. H. Sun, EPRI Program Manager for his stimulating discussion and his assistance in locating some of the relevant references.

REFERENCES

1. K. H. Sun, R. B. Duffey and C. M. Peng, The prediction of two-phase mixture level and hydrodynamically-controlled dryout under low flow conditions *Int. J. Multiphase Flow* **7**, 521–543 (1981).
2. Nuclear Safety Analysis Center Staff, *Analysis of the Three Mile Island Unit-2 accident*, Electric Power Research Institute, EPRI-NSAC-1, Report No. 1, July (1979) Supplement, October (1979).
3. J. N. Reyes, Jr., Radiative heat transfer to high pressure steam, ASME Paper 81-HT-69, 20th National Heat Transfer Conference, Milwaukee, Wisconsin, August (1981).
4. G. R. Thomas and B. Chexal, *Zirconium oxidation during high-pressure-temperature, steam-depleted conditions*, Electric Power Research Institute, EPRI-NSAC Report No. 29, July (1981).
5. Private communication from Dr K. H. Sun, 20 February (1981).
6. B. T. Chao, S. J. Chen and L. S. Yao, *Heat and mass transfer in laminar boundary layers over a vertical Zircaloy plate with hydrogen generation*, Electric Power Research Institute, EPRI RP 1762-2, Final Report, December (1981).
7. P. H. Oosthuizen and R. Hart, A numerical study of laminar combined convective flow over flat plates, *Trans. Am. Soc. Mech. Engrs*, Series C, *J. Heat Transfer* **95**, 60–63 (1973).
8. G. Wilks, Combined forced and free convection flow on vertical surfaces, *Int. J. Heat Mass Transfer* **16**, 1958–1963 (1973).
9. S. J. Chen, B. T. Chao and L. S. Yao, Free convection over a vertical Zircaloy plate in steam with simultaneous oxidation, *Proc. 7th Int. Heat Transfer Conf.*, Munich, Germany, Paper No. NR4 (1982).
10. C. L. Tien and J. G. Munthe Andersen, Radiation heat transfer in a BWR fuel bundle under LOCA conditions, in *Fluid Flow and Heat Transfer over Rod or Tube Bundles* (edited by S. C. Yao and P. A. Pfund). ASME G00157 (1979).
11. P. A. Lottes, *Nuclear reactor heat transfer*, Argonne National Laboratory, ANL-6469, pp. 67–69 December (1961).
12. C. R. Wilke, A viscosity equation for gas mixtures, *J. Chem. Phys.* **18**, 517 (1950).
13. Y. S. Touloukian, R. W. Powell, C. Y. Ho and M. C. Nicolaou, *Thermophysical Properties of Matter: Viscosity*, Vol. 11, IFI/Plenum, New York (1973).
14. E. A. Mason and S. C. Saxena, Approximate formula for the thermal conductivity of gas mixture, *Phys. Fluids* **1**, 361–369 (1958).
15. R. C. Reid, J. M. Prausnitz and T. K. Sherwood, *The Properties of Gases and Liquids*. McGraw-Hill, New York (1977).
16. W. M. Kays, *Convective Heat and Mass Transfer*. McGraw-Hill, New York (1966).
17. T. Fujii and M. Fujii, The dependence of local Nusselt number on Prandtl number in the case of free convection along a vertical surface with uniform heat flux, *Int. J. Heat Mass Transfer* **19**, 121–122 (1976).
18. W. B. Hall and P. H. Price, Mixed forced and free convection from a vertical heated plate to air, *Heat Transfer*, 1970, *4th Int. Heat Transfer Conf.*, Paris-Versailles, Vol. IV, Paper NC 3.3 (1970).

CONVECTION MIXTE SUR UNE PLAQUE VERTICALE EN ZIRCALOY DANS LA VAPEUR D'EAU ET AVEC OXYDATION SIMULTANEE

Résumé—On étudie analytiquement l'écoulement de couche limite, laminaire permanent d'un mélange de vapeur d'eau et d'hydrogène sur une plaque verticale en Zircaloy dans les conditions de l'accident du réacteur nucléaire de Three Mile Island. La loi de croissance de l'oxydation expérimentalement observée est modifiée tenir compte de la présence possible de l'hydrogène dans la vapeur hors de la couche limite et pour des températures variables de la plaque. L'oxydation du Zircaloy donne lieu à une faible vitesse de succion du mélange vapeur–hydrogène à la surface. Des détails des profils des composants de la vitesse, de température et de concentration d'hydrogène dans la couche limite sont présentés aussi bien que les distributions longitudinales de la vitesse de succion pariétale, du frottement pariétal et de la température pariétale. Une étude paramétrique de la perte par rayonnement est faite en utilisant des données récentes sur le coefficient de rayonnement. Des formules sont proposées pour l'élévation de la température locale de la paroi et pour les nombres locaux de Nusselt et de Sherwood.

MISCHUNGSKONVEKTION AN EINER SENKRECHTEN ZIRKALOY-PLATTE IN DAMPF BEI GLEICHZEITIG STATTFINDENDER OXIDATION

Zusammenfassung—Es wird eine analytische Untersuchung des quasistationären und laminaren binären Dampf-Wasserstoff-Stromes an einer senkrechten Zirkaloy-Platte durchgeführt; dabei entsprechen die Bedingungen denen während des Unfalls im Kernkraftwerk Three Mile Island. Die experimentell beobachtete Gesetzmäßigkeit der Oxidationsrate wird erweitert, um möglicherweise außerhalb der Grenzschicht vorandenen Wasserstoff und verschiedene Plattentemperaturen zu berücksichtigen. Die Oxidation des Zirkaloy führt zu einer kleinen Sauggeschwindigkeit des Dampf-Wasserstoff-Gemisches in Richtung der Metall-Oberfläche. Längs- und Querkomponenten von Geschwindigkeitsprofil, Temperatur und Wasserstoffkonzentration in der binären Grenzschicht werden im einzelnen dargestellt, ebenso die Verteilung der Sauggeschwindigkeit, Wandschubspannung und Wandtemperatur längs der Oberfläche. Eine Parameterstudie über den Einfluß der Wärmeverluste der Wand durch Strahlung wurde ebenfalls durchgeführt, wobei kürzlich veröffentlichte Angaben über den Wärmeübergangskoeffizienten durch Strahlung benutzt wurden. Beziehungen für den Anstieg der örtlichen Wandtemperatur und die örtlichen Nusselt- und Sherwood-Zahlen werden vorgeschlagen.

СМЕШАННАЯ КОНВЕКЦИЯ НАД ВЕРТИКАЛЬНОЙ ЦИРКАЛОЕВОЙ ПЛАСТИНОЙ В ПОТОКЕ ПАРА ПРИ ОДНОВРЕМЕННОМ ОКИСЛЕНИИ

Аннотация—Проведено теоретическое исследование квази-стационарного ламинарного бинарного течения пара и водорода в пограничном слое над вертикальной циркалоевой пластиной при условиях, имевших место при аварии ядерного реактора на Три-Майл Айленд. Наблюдаемый в экспериментах закон скорости окисления модифицирован таким образом, чтобы учитывать возможное присутствие водорода в паре за пределами пограничного слоя и переменную температуру пластины. Окисление циркалоя вызывает небольшую скорость всасывания пароводородной смеси у поверхности кожуха. Приведены как продольные и поперечные компоненты профилей скорости, температуры и профили концентрации водорода поперек бинарного пограничного слоя, так и продольные распределения скорости всасывания у стенки, пристеночного сдвига и температуры стенки. Проведено параметрическое исследование влияния поверхностных радиационных потерь тепла, в котором использованы последние данные о коэффициенте радиационного теплообмена. Предложены соотношения для местного повышения температуры стенки и локальных чисел Нуссельта и Шервуда.